

DESIGN REPORT

KAGRA photon calibrator

Author:

Yuki INOUE, Sadakazu Haino, Nobuyuki Kanda
on the behalf of Calibration sub-group

KAGRA
Calibration subsystem

February 22, 2017



Abstract

KAGRA
Calibration subsystem

KAGRA photon calibrator

by Yuki INOUE, Sadakazu Haino, Nobuyuki Kanda
on the behalf of Calibration sub-group

Accurate calibration of the output of the Gravitational Wave (GW) signal is crucial to determine the physics parameters of the sources. The primary tools used in the advanced GW detectors are photon calibrators based on the radiation pressure. In this document, we report the design of the KAGRA photon calibrator in order to achieve the absolute accuracy of 1% to meet the calibration requirements of second-generation GW detectors in the new era of GW astronomy.

Acknowledgements

We thank LIGO Pcal team lead by Prof. Rick Savage of LIGO Hanford Observatory who strongly encouraged and supported this work by sharing all the technical details and giving numerous critical comments and suggestions.

We should add Jeff Kissel, Darkhan Tuyenbayev, Peter King, Kiwamu Izumi, Evan Goetz, Sudarshan Karki, Wang-Yau Cheng, Tomotada Akutsu, Kentaro Somiya, Kimura Nobuhiro, Lin Chih-hsun, Ayako Ueda, Ayako Hagiwara, Yoshikazu Nama, Shinichi Terashima, Kazudhiro Kazuhiko, Yoshio Saito, Kumar Rahul.

KAGRA project is supported by MEXT and JSPS in Japan as well as its collaborating institutes. YI and SH acknowledge the supports by Academia Sinica and MoST in Taiwan.

Contents

Abstract	iii
1 Introduction	1
1.1 Calibration of a Gravitational-Wave detector	1
1.2 Roles of the photon calibrator	2
1.3 Schedule of KAGRA	3
1.4 Calibration requirements from data analysis	3
2 Photon calibrator	5
2.1 Photon calibrator	5
2.2 Purpose of photon calibrator	5
2.2.1 Interferometer Calibration	5
2.2.2 Hardware injection test	5
2.2.3 Photon pressure actuator	5
2.3 Calibration line of KAGRA	5
3 Instruments descriptions	7
3.1 Layout of Photon calibrator	7
3.2 Transmitter (Tx) module	7
3.2.1 Fiber laser	10
3.2.2 Beam shutter	10
3.2.3 Half wave plate	10
3.2.4 Polarizer	10
3.2.5 Lens	10
3.2.6 Mirror	12
3.2.7 Optical mount with Pico-motor	12
3.2.8 Beam splitter	13
3.2.9 Optical follower servo	13
3.2.10 Photo detector	15
Cover	15
InGaAs detector	15
Electrical Circuit	16
3.2.11 Beam sampler	16
3.2.12 2 inch integrating sphere	16
3.2.13 Structure	16
3.3 Periscope	16
3.3.1 Geometric optics	17
3.3.2 View window	17
3.3.3 Mirrors	19
3.3.4 Structure	20
3.3.5 Alignment	20
3.4 Receiver module	20
3.4.1 6inch Integrating sphere	20

3.4.2	Mirror	20
3.4.3	QPD	20
3.4.4	Structure	21
3.5	Camera module	21
3.5.1	Camera	21
3.5.2	Telescope	21
3.5.3	Focuser	22
3.5.4	View window	22
3.5.5	Mirror	22
3.5.6	Illuminator	23
3.6	Summary	23
4	Elastic deformation	25
4.1	Free mass motion	25
4.2	Transfer function	25
4.3	Modal analysis	25
4.4	Elastic deformation	25
4.5	Summary	25
5	Absolute power calibration	27
5.1	Introduction	27
5.2	Theory of Operation	27
5.3	End-station	27
5.4	Gold standard	27
5.5	Working standard	27
6	Beam position monitor	29
7	Discussion	31
8	Summary	33
	Bibliography	35

Chapter 1

Introduction

1.1 Calibration of a Gravitational-Wave detector

KAGRA is a laser interferometer using four mirrors (test masses) suspended from multi-stage pendula to form two perpendicular optical cavities (arms). Gravitation Wave (GW) strain causes differential variations of the arm length and generates power fluctuations in the detector readout port. The power fluctuations measured by photodetectors work as the GW readout signal and an error signal to control the differential arm length. For the stable operation of the instrument, a feedback control of the differential arm length is required. This control is achieved by taking a digitized readout signal, applying a set of digital filters, and sending the control signal to the test mass actuators. Therefore, estimation of the equivalent GW strain sensed by the interferometer requires detailed characterization and correction for the feedback control loop.

The calibration uncertainties are directly translated to the systematic errors on the absolute GW signal amplitude. In case of LIGO GW150914 event, the calibration was established to an uncertainty (1σ) of less than 10% in amplitude and 10 degrees in phase [1]. In case of LIGO GW151226 event, the calibration uncertainty (1σ) in both detectors at the time of the signal is better than 8% in amplitude and 5 degrees in phase [2].

The primary impact of the calibration uncertainties to the physics parameters is the determination of the distance to the source. The 10% uncertainties of the GW amplitude directly correspond to 10% uncertainties on the estimation of the luminosity distance. Furthermore, since the estimation of the population of the GW sources depends on the third power of the source distance, 10% calibration uncertainties will be translated into $\sim 30\%$ uncertainties on the population estimation.

The calibration uncertainties also affect the coordinate reconstruction particularly in the case that only up to three detectors in the world GW detector network can detect the GW signal. This can often happen because the sensitivity of interferometer has directional dependence. The effect of calibration uncertainties is visible at high signal-to-noise ratio events where the angular resolution is less affected by the detector noise. In such cases, the pointing accuracy can get worse by factor of $2\sim 4$ with 10% calibration uncertainties [3].

1.2 Roles of the photon calibrator

Photon calibrators are the primary calibration tools in the Advanced LIGO and Advanced Virgo detectors [4–6]. Earlier versions have been tested on various interferometers [7–9], and they have evolved significantly in LIGO over the past ten years [10]. There are several unique roles required to the photon calibrator:

1. Check of the sign of $h(t)$

Since the direction of the movement of test mass is proportional to the laser power, photon calibrator allows a direct check of the sign of the reconstructed $h(t)$ channel compared to the definition taken in agreement with other experiments. In initial phase of Virgo, the primary purpose of photon calibrator was to check the sign of $h(t)$ [11].

2. Calibration during the observing periods

Calibration methods without using photon calibrator such as using radio-frequency oscillator and laser wavelength can be done only under the limited condition where the interferometer is not operating in the optimum sensitivity. The propagation of calibration parameters from the high noise condition to the low noise condition can introduce additional unknown source of systematic errors. On the other hand, the photon calibrator is a completely independent instrument of the interferometer and therefore can actuate the test masses during the observation periods with optimum sensitivity.

3. Hardware injection

Hardware injection in the high frequency region is important to verify the response of the detector system. Since actuators are inside the feedback control loop, the amplitude is more suppressed for higher frequencies. Photon calibrator can inject the high frequency signal more efficiently.

4. Independence of calibration method and reliability assurance of interferometer

Injecting calibration signals into the control feedback loop has a limitation to reduce the systematic errors because it is calibrating the loop itself. Without Pcal, it is difficult to disentangle each uncertainty inside the loop, such as optical gain and actuator efficiency. On the other hand, Pcal has a strong advantage to enable to inject calibration signals independent of the control loop and provide an additional way to reduce the systematic uncertainties.

5. Globalization of the calibration

It is necessary to calibrate and compare the absolute accuracies of KAGRA, LIGO and Virgo, or at least we need to have a way to evaluate the difference of absolute GW amplitude between different detectors. This kind of difference introduces bias on the physics parameters such as the source localization. Typical examples are cosmic-ray air shower observations and X-ray observations. In the long history of the air shower experiments, there have been always discussions about the absolute energy estimation. On the other hand, X-ray detector can be calibrated by the radio isotope sources and there is no question raised. In the GW experiment, absolute calibration is a difficult work but therefore it will be the key issue of the experimental verifications in the next decades.

1.3 Schedule of KAGRA

In order to coincide the observation plan by LIGO and Virgo [12], KAGRA is currently installing the instrument to meet the following observation schedule [13]:

1. Phase-1: 2017.3 – 2018.3
Operation of Michelson interferometer in cryogenic condition followed by introducing Fabry Pérot cavity.
2. Phase-2: 2018.4 – 2019.3 (Opening)
Full lock of RSE (Resonant Sideband Extraction)
3. Phase-3: 2019.4 – 2020.3 (Early)
One year commissioning after the first full operation, then improve the sensitivities to achieve the design goal
4. 2020 – 2021: Middle term observation
5. 2021 – 2022: Late term observation
6. 2022 – : Observation with the designed sensitivity

1.4 Calibration requirements from data analysis

Chapter 2

Photon calibrator

2.1 Photon calibrator

One of the goals of the gravitational wave experiment is the accurate measurement of the gravitational waveform that is measured through the absolute displacement of the end test masses. A recent study that LIGO conducted in US showed that a displacement uncertainty could be controlled by the photon calibrator. The photon calibrator is one of the calibration tools to push the mirror surface using the photon pressure of the laser as shown in Fig XXX. The absolute displacement is described as

$$dx = \frac{P \cos \theta}{c} s(f) \left(1 + \frac{I}{M} \vec{a} \cdot \vec{b} \right), \quad (2.1)$$

where P is an absolute power of the laser, c is the speed of light, θ is an incident angle of the laser, I and M are moment of inertia and mass of test mass, \vec{a} and \vec{b} is position vector of photon calibrator lasers and interferometer laser. Then, $s(f)$ is transfer function of the test masses. We simulated the transfer function of test mass as shown in Fig. XXX. We assumed the masses, shapes and Young's modules of the each pendulum mass and fiber as shown in Fig.XXX. According to transfer function, we can regard the motion of high frequency as free mass due to higher than the natural frequency. Therefore, we are able to assume as follows:

$$s(f) = \frac{1}{M\omega^2}, \quad (2.2)$$

where ω is the angular frequency of test mass.

2.2 Purpose of photon calibrator

- 2.2.1 Interferometer Calibration
- 2.2.2 Hardware injection test
- 2.2.3 Photon pressure actuator

2.3 Calibration line of KAGRA

Chapter 3

Instruments descriptions

3.1 Layout of Photon calibrator

The KAGRA photon calibrator is placed around EXA/EYA chamber, which is installed 36 m away from the end test mass (ETM). We push the mirror surface with the modulated photon pressure directly. Figure 3.1 shows the layout of the KAGRA photon calibrator. The photon calibrator consists of transmitter module (Tx module), receiver module (Rx module), periscope, and telephoto camera module (TCam module). We place the 20 W laser in Tx module, whose frequency is 1047 nm. The 1064 nm laser is not used due to avoid the coupling with main beams. The power of the laser is modulated by the optical follower servo (OFS). We split the beams in Tx module for pushing the drum head node points of the ETM due to elastic deformation. We transfer the beams to the ETM though the periscope. All the periscope structures are placed into the EXA/EYA chamber. The beam is received by the Rx module. We place a 6 inches integrating sphere for the accurate measurement of the laser power and two quadrant photo detector (QPD) for the beam position monitor. We also measure the beam position on the ETM surface using the telephoto camera (TCam). The Tcam is consists of the astronomical telescope, focuser, and high resolution digital camera. Details of instruments are described following section.

3.2 Transmitter (Tx) module

The Tx module is placed at the side of the EXA/EYA chamber. Figure 3.2 shows the view of Transmitter module. All the optical components are mounted on the 900 mm × 900 mm breadboard (B9090L; Thorlabs). The bread board is placed on the support structure. The electrical module for the control and readout are also hosed in the support structure.

Figure 3.3 shows the optical layout of Tx module. All the optical components are listed in Table 3.1.

TABLE 3.1: .

#	Name	Type
1	Fiber laser	CYFL-TERA-20-LP-1047-AM1-RGO-OM1-T305-C1

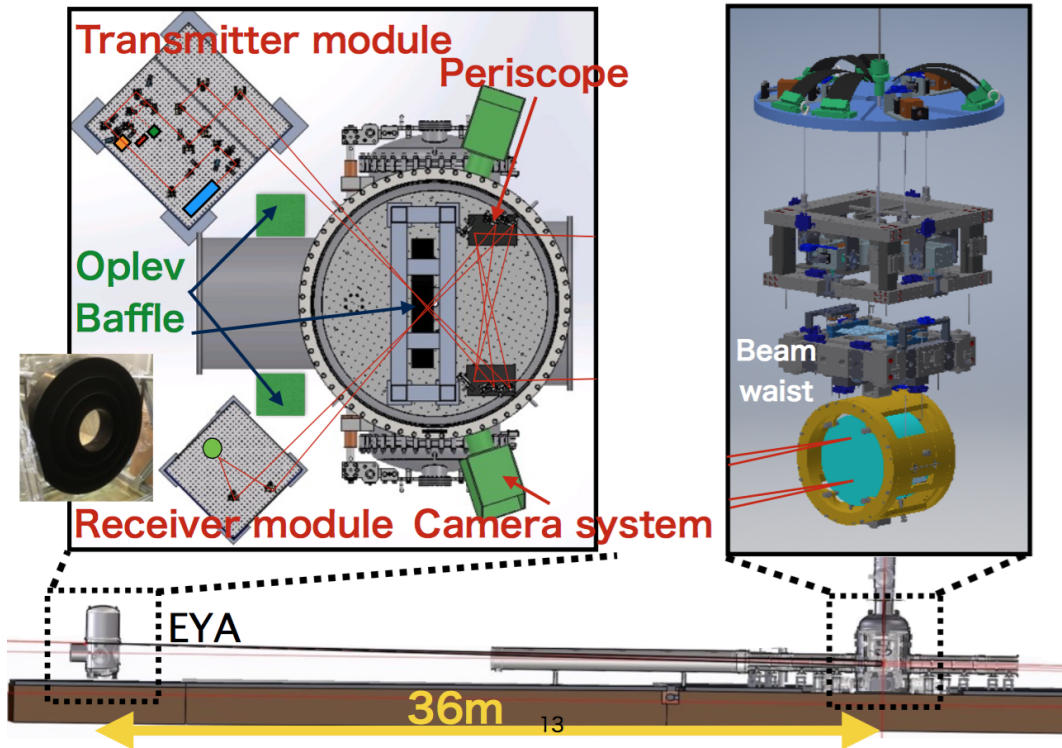


FIGURE 3.1: KAGRA photon calibrator. The calibration system is placed around the EXA/EYA chamber. We mount the optical lever and optical baffle as well.

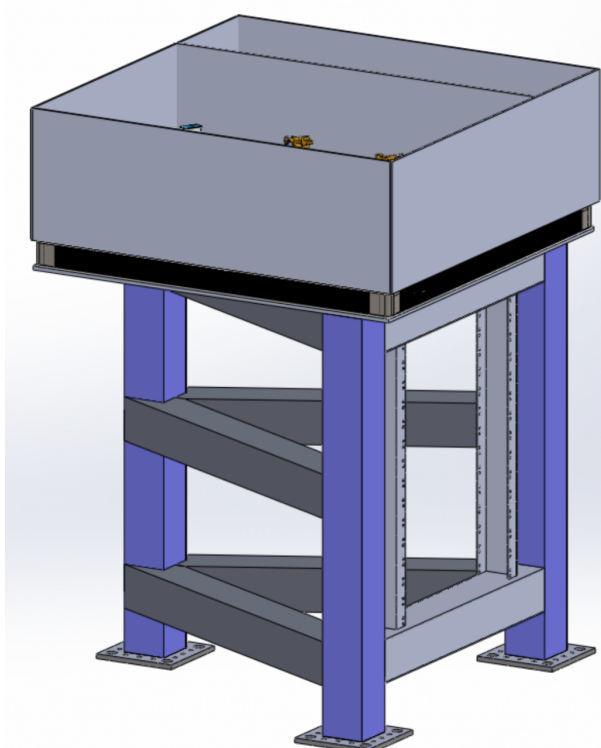


FIGURE 3.2: Transmitter module of KAGRA Pcal. We place the optical table on the triangle table. The readout and control device is housed into the legs of table.

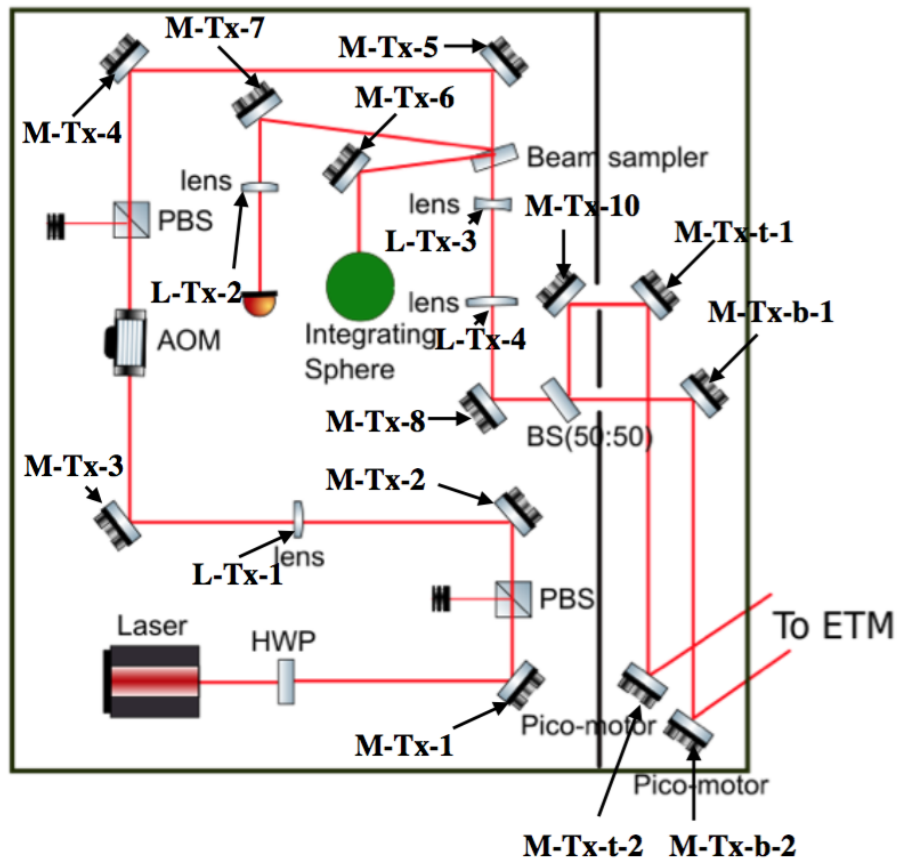


FIGURE 3.3: Optical layout of KAGRA photon calibrator. The laser power is modulated and controlled by the acousto-optic modulator (AOM). This modulated laser is sent to a 50:50 beam splitter, where we monitor the modulated laser power by using the integrating sphere.

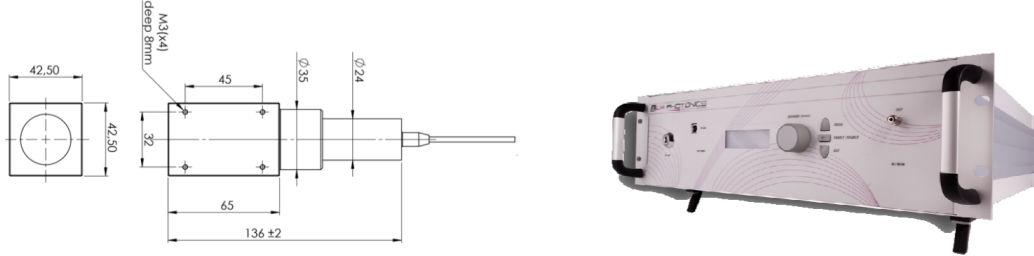


FIGURE 3.4: The fiber laser and drawing of isolator.

3.2.1 Fiber laser

We employ the CW fiber laser made by the LER photonics as shown in Fig. 3.4. The maximum power and frequency are 20 W and 1047 nm, respectively. The model number of the laser is CYFL-TERA-20-LP-1047-AM1-RGO-OM1-T305-C1. The maximum laser power of KAGRA Pcal is 10 times larger than that of LIGO. This is because that we need the high power laser for the injection test and photon pressure actuator technique. The typical beam width of the laser is 0.5 mm when we mount the isolator. We summarize the specification of the laser as shown in Table 3.2.

3.2.2 Beam shutter

We have to pay attention to safety for the operation of the high power laser. In order to dump the beam, we use the beam shutter made by lasernet company. The model number of the shutter is LS-10-12. The aperture size and Max laser power are 15 mm and 20 W. These number meet our requirement due to the laser spot size and maximum power. We control the beam shutter on the GUI. The specification of the beam shutter is shown in Table 3.3.

3.2.3 Half wave plate

To control the polarization angle of incident beam, we employ the zero order half wave plate (HWP) made by the CVI laser optics. The model number of the HWP is QWPO-1047-05-2-R10 whose diameter are 12.7mm. The HWP is mounted on the rotation mount made by Thorlabs. The thick ness are optimized at 1047 nm. The specification of the HWP is listed in Table 3.4.

3.2.4 Polarizer

We place two polarizers to define the polarization angle accurately. This is because that the power of the laser is modulated by acousto-optic modulator (AOM) whose performance strongly depend on the incident polarization angle. One polarizer is placed behind HWP. Another one is placed after AOM. The Polarizer is made by Karl-Lamrecht. We purchased TFPC12-1047 that is optimized at 1047 nm.

3.2.5 Lens

We have dane a mode matching simulation using JamMt. We assumed laser beam to be gaussian distribution. We have to place the focus of the laser at the AOM. Thus, we decide the optimal position and focal length of the 1 inch lens (L1), where the

TABLE 3.2: Specification summary of CW fiber Laser.

Characteristic	Typical value	Unit	Note
Operating central wavelength	1047	nm	± 1 nm
CW output power	20	W	
Output signal line-width	0.5	nm	FWHM
Output power stability	± 1	%RMS	Output power: 20 W
Output power tunability	10-100	%	
Optical polarization	Linier		
Polarization extinction ratio	15	dB	
Output fiber	PLMAFUD3460		Nufurn company
Output fiber length	2	m	
Beam diameter	0.5	mm	with isolator
Beam quality	1.1	M^2	
Control mode	Active current control, Active power control		
Beam quality	1.1	M^2	
Supply voltage	84-264	V	AC 47 to 63 Hz
Power consumption	650	W	
Housing	448x451x132.5	mm	
Total weight	13	kg	
Cooling	Air cooled with fans		
Operating temperature	15-35		
Humidity	5-85	%	

TABLE 3.3: Specification of beam shutter.

Characteristic	Typical value	Unit	Note
Max laser power	20	W	
Aperture size	15	mm	
Drive voltage	11-14	V DC	
Current consumption	150	mA	
Size	98 × 63.5 × 36	mm	

TABLE 3.4: Specification of HWP.

Characteristic	Typical value	Unit	Note
Waveplate Type	Quartz Waveplates		
Wavelength Range	1047	nm	
Retardance	$\lambda/2$		
Clear Aperture	85	%	of diameter
Reflection	0.25	%	
Retardance Tolerance	$\lambda/200$ to $\lambda/500$		at 23Degree C
Material	Crystal Quartz		
Surface Quality	10-5	scratch-dig	
Waveplate Diameter	12.7	mm	

TABLE 3.5: Specification of lenses.

Lens number	part number	Diameter [mm]	Focal length
L1		25.4	
L2		25.4	
L3		25.4	
L4		50.8	

assumed beam waist of the fiber laser and AOM are 0.5 mm and XXX mm, respectively. Furthermore, we place two lenses for placing the focus at the surface of the ETM. We employ the combination of 1 inch negative lens and 2 inch positive lens. The Gaussian beam can describe the following relation:

$$w(z) = \omega_0 \sqrt{1 + \left(\frac{\lambda z}{\pi \omega_0^2} \right)^2}, \quad (3.1)$$

where λ is wavelength of the laser, w_0 is beam waist, z is direction from the focus. We estimate the minimum differential beam spot by changing beam waist because it make the alignment easier. The minimum beam spot is written by

$$\left. \frac{dw(z)}{dw_0} \right|_{z=36m} = 0. \quad (3.2)$$

The estimated beam waist and beam spot is 3.5 mm and 5.5 mm as shown in Fig. XXXX. We also place the lens at the front of the photo detector for the OFS. The parameters of the simulation results are listed in Table. 3.5. All lenses are made by CVI laser optics. The material of lenses are fused silica. The AR coating is placed at both surface.

3.2.6 Mirror

We employ nine 1 inch mirrors and four 2 inch mirrors. The 1 inch mirror is made by CVI laser optics. They place the HR coating on the surface of mirror. On the other hand, we use the HR coating on the fused silica disc of 2 inch in diameter. The coating and polishing the fused silica is made by Sigma-koki corporation. The reflectance of the mirror is shown in Fig. 3.3. The reflectance of HR coating depends on the incident angle and the polarization angle. We labeled mirrors as M-Tx1 to M-Tx-11, M-Tx-t-1, M-Tx-t-2, and M-Tx-b-1. The specification of mirrors are summarized in Table.3.6. All mirror is aligned with optical mirror mount made by Newport company.

3.2.7 Optical mount with Pico-motor

The uncertainty of the beam position on the ETM is one of the largest. To control the beam position, we employ the Pico-motor after flip mirrors for changing mirror angle. The pico-motor is made by New port, whose part number is 8822.

TABLE 3.6: Specification of Mirrors.

Mirror number	part number	Diameter [mm]	Incident angle	Polarization
M-Tx-1		25.4	45	
M-Tx-2		25.4	45	
M-Tx-3		25.4	45	
M-Tx-4		25.4	45	
M-Tx-5		25.4	45	
M-Tx-6		25.4	48	
M-Tx-7		25.4	42	
M-Tx-8		25.4	45	
M-Tx-9		25.4	45	
M-Tx-10		50.8	45	
M-Tx-t-1		50.8	45	
M-Tx-t-2		50.8	23.3	
M-Tx-b-1		50.8	45	
M-Tx-b-2		50.8	21.8	

3.2.8 Beam splitter

To reduce the elastic deformation, we separate the beam with the beam splitter made by CVI laser optics for pushing the node points of mirror. The part number of beam splitter is BS1-1064-50-2025-45P. The diameter of the beam splitter is 2 inch. Table 3.7 shows the separation ratio of beam splitter.

3.2.9 Optical follower servo

In order to achieve low-noise and accurate modulation, an active controller (servo) can modulate the waveform by means of feedback control. This feedback loop used for the Pcal is called as the Optical Follower Servo (OFS). The OFS will be used in the KAGRA Photon Calibrator as a means to reduce the relative power noise (RPN) of the laser. We will achieve maximum sideband to carrier suppression of the modulated output waveform. The block diagram of the OFS is shown in Fig. XXX. The transfer function of this diagram can be described as

$$\frac{AG_1}{1 + AKSG_1G_2}, \quad (3.3)$$

where A is actuation factor, S is sensing factor, K is percentage of light power sampled, G_1 and G_2 are gain of feedforward and feedback.

We monitor the difference between input and feed back signal at the error point. For monitoring the performance of OFS, we read the location of monitor point. When we inject the signal, such as swept sine, gauss sine and hardware injection signal, we use input port. The estimation of the expected gain parameter is listed in Table 3.8.

The KS corresponds to the trans impedance gain of detector. The detail of photo detector is described in Sec.3.2.10. According to Table. 3.8, we regard G_2KS as unity. Therefore, we can simplify the transfer function as follows:

$$\frac{AG_1}{1 + AG_1} \quad (3.4)$$

TABLE 3.7: Specification of beam splitter.

Characteristic	Typical value	Unit	Note
Beamsplitter Type	Laser Line Plate Beamsplitters		
Beamsplitter Shape	Round		
Wavelength Range	800	nm	
Bevel/Chamfer	0.35 mm × 45 Degree		
Wedge Angle Tolerance	5	arcmin	
Coating Material	Laser Line Dielectric		
Angle of Incidence	45	Degree	
Clear Aperture	85	%	
Substrate/Material	Fused Silica		
Surface Flatness	$\lambda/10$		
Surface Quality	10-5	scratch-dig	
Beamsplitter Diameter	50.8	mm	
Beamsplitter Thickness	6.35 mm		
Thickness Tolerance	± 0.25 mm		

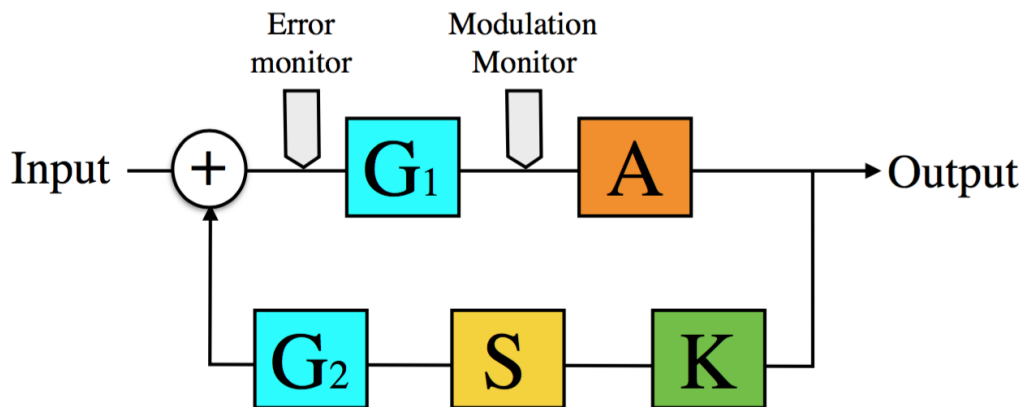


FIGURE 3.5: r.

TABLE 3.8: OFS gain.

	Gain	unit
A	0.5	W/V
G_1	10-100	V/V(dB)
G_2	2	V/V(dB)
KS	0.5	V/W

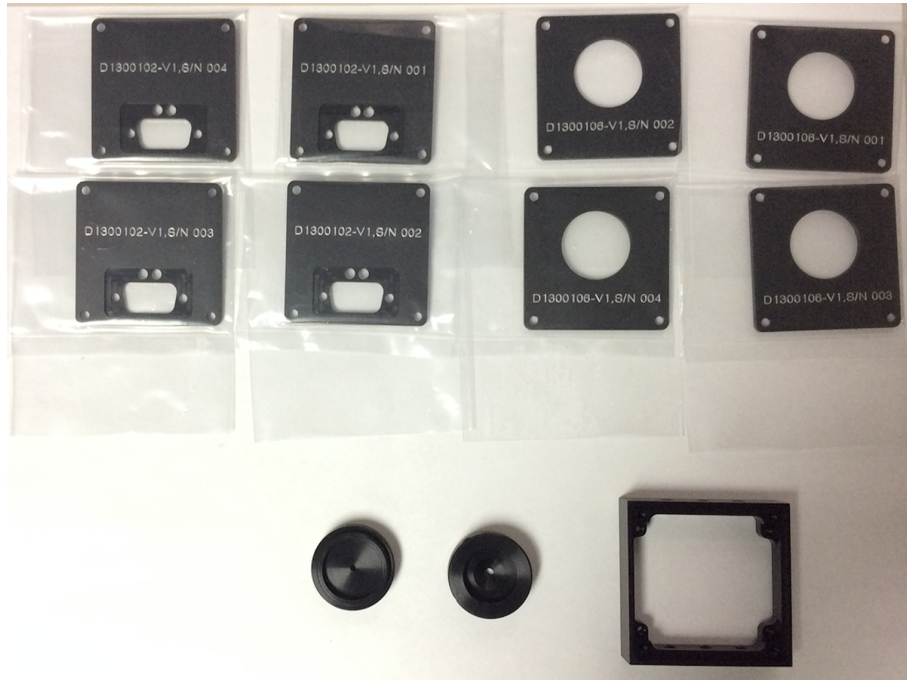


FIGURE 3.6: .

We require the band width of OFS much larger than operation frequency. We employ the AOM as modulator, which made by ISOMET. The part number of AOM is M1080-T80L-M.

3.2.10 Photo detector

To detect the laser power, we use the photo detector. We place the photodetector at the working standard, Optical follower servo, Integrating sphere in Tx and Rx module. We developed the photo detector as shown in Fig.3.6. We employ the InGaAs photo diode for absolute power measurement. The InGaAs diode is placed on the circuit board. The beam is collimated for the power detection reasonably.

Cover

The design of the cover is done by LIGO Pcal group. We make the detector cover in Academia Sinica, Institute of Physics. Figure 3.6 shows the machined detector covers. We housed the circuit board into the cover coated by the black anodized aluminum.

InGaAs detector

We employ the C30665GH, large area InGaAs PIN photodiode with diameter of 3.0 mm with a flat glass window. The C30665GH provides high quantum efficiency from 800nm to 1700nm. This detector is fabricated by Excelitas. The specification of detector is shown in Table 3.12.

ditector

TABLE 3.9: Specification of InGaAs detector.

Characteristic	Typical value	Unit	Note
Dark Current	25	nA	
Peak Wavelength	1550	nm	
Responsivity	0.95	A/W	
Breakdown Voltage	50	V	
Capacitance	200	pF	



FIGURE 3.7: .

Electrical Circuit

We newly improved the electrical circuit of the photon detector as shown in Fig. 3.7. The electrical circuit is housed in the aluminum cover. We place the photo detector at the the behind of the electrical circuit. The layers of the circuit consists of 4 layer. We change the differential gain by changing the register and capacitor of the circuit. The electrical circuit are shown in Fig. 3.8.

3.2.11 Beam sampler

3.2.12 2 inch integrating sphere

The 2 inches integrating sphere is used for absolute power measurement of the laser. We receive the separated laser beam at beam sampler. We mount the photo detector at the port of integrating sphere. The integrating sphere is made by the Lab sphere. The inner surface of the integrating sphere in mounted on the Spectralon.

3.2.13 Structure

The breadboard is placed on the support structure. The material of this structure is SUS 306. This structure can be housed electrical devices, such as driver of the fiber laser, electronics of optical follower servo, and driver of laser shutter. We simulated the resonance frequency using ANSYS. The estimated frequency is XXX Hz.

3.3 Periscope

The periscope is used for sending the beams to ETM. We place the periscopes in EXA/EYA chamber as shown in Fig. 3.9. They consist of four periscopes. The first periscope is mounted at the vacuum side of the window. The laser is send to second

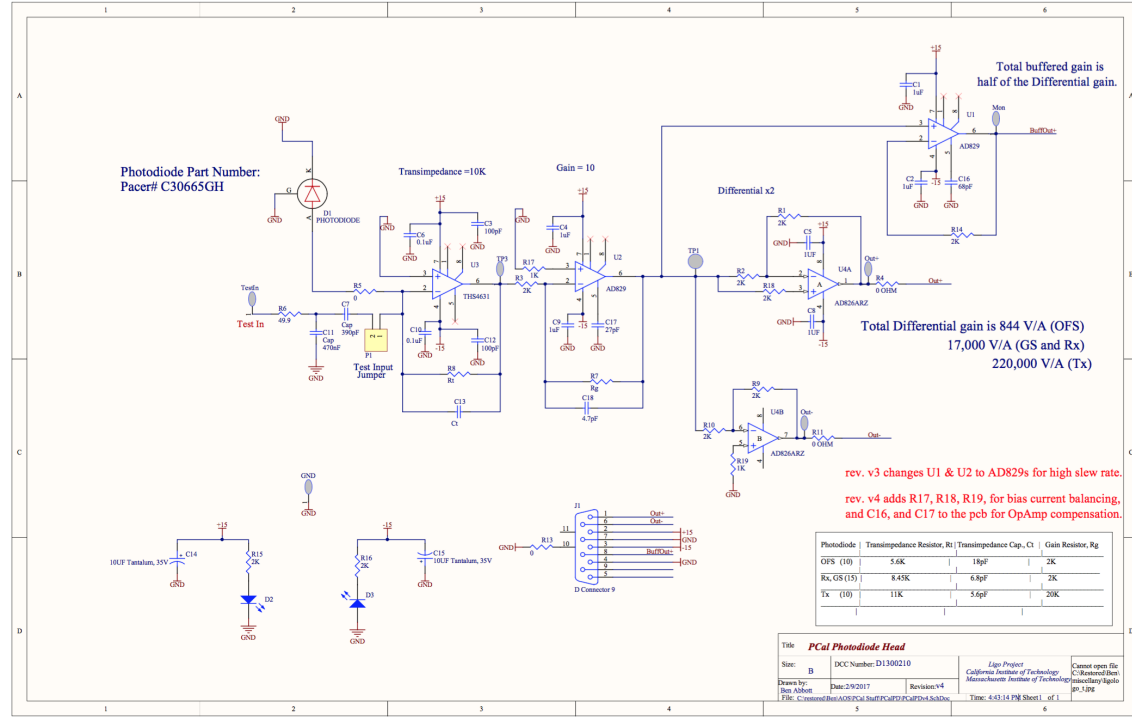


FIGURE 3.8: D1300210.

periscope on optical table. We share one first mirror and one second mirror for the two beams of the laser. We send the two laser to two third periscope. The third periscope is sent to fourth periscope, which is aligned to same hight of the injected beam to the ETM.

3.3.1 Geometric optics

We consider the beam separation and focus position of the optical system for the laser to be sent and received to the ETM. We fixed 80 mm separation of the mirror in transmitter module. Figure 3.10 shows the schematic view of optical layout, where D_{win} , D_{m2} , and D_{m3} are separation of beams, L_{win} , L_{m2} , and L_{m3} are distance of each components. We calculated the beam separation of the vacuum window, second mirror, and third mirrors by changing the focus point as shown in Fig. 3.11. X axis shows the distance from the window. We find a optimal point of minimum separation of the window because of clear aperture of window and second mirror. The optimal focus point is at 370 mm from the window corresponding to 108 mm separation of the mirror. We also find a incident angle of window with optimal focus point as 1.6 degree.

3.3.2 View window

One of the serious systematic errors are optical efficiency of the view port. Therefore, we have to reduce the reflectance of view port at least 0.1 %. We employ the fused silica optical window whose diameter and thickness are 100 mm and 0.5 inch. We place the AR coating on both surfaces of the window. Figure XXX shows the simulated transmittance of the view port. The effective diameter of the view port is about 3 inch. The incident angle of the beams are 1.6 degree. We mounted the first

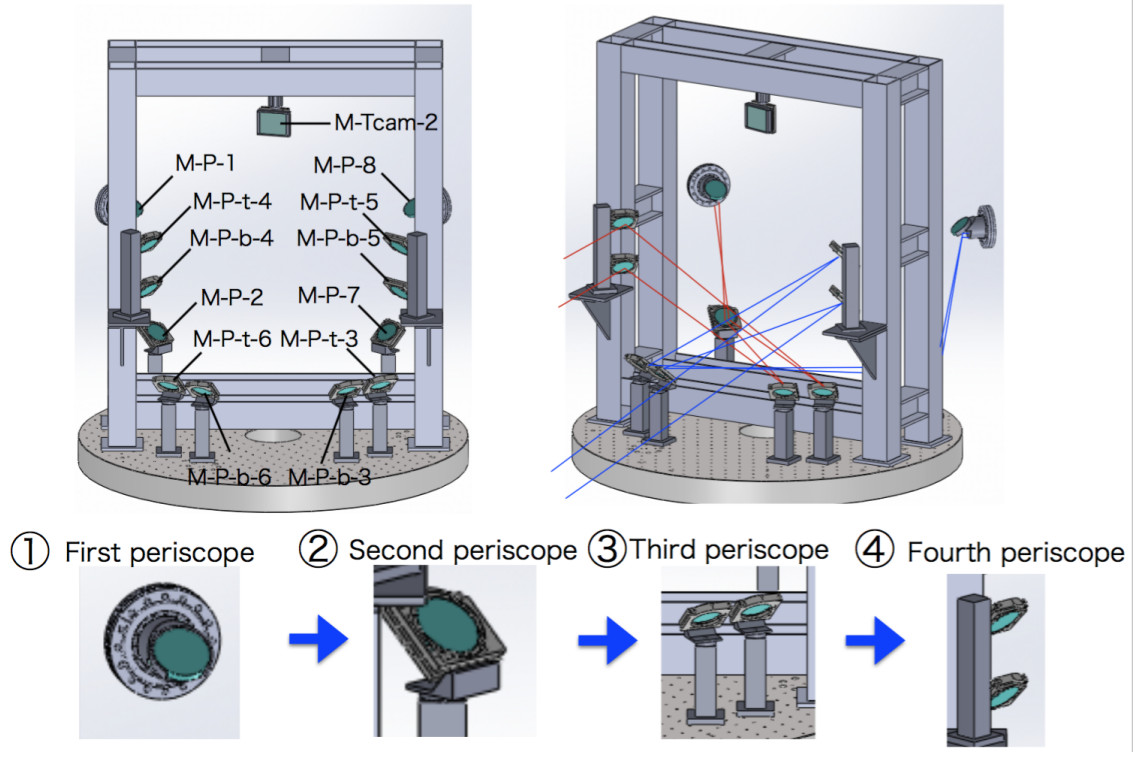


FIGURE 3.9: Periscope.

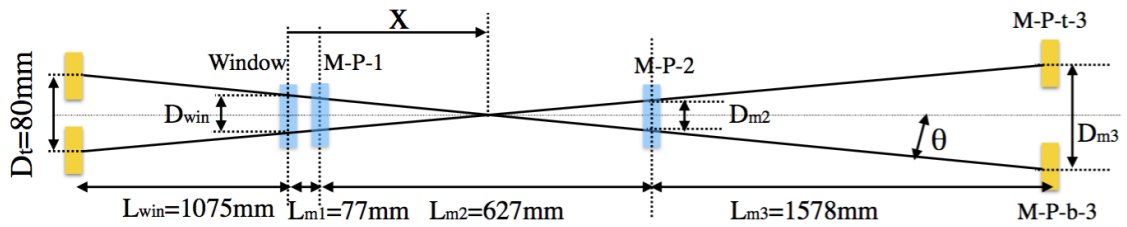


FIGURE 3.10: .

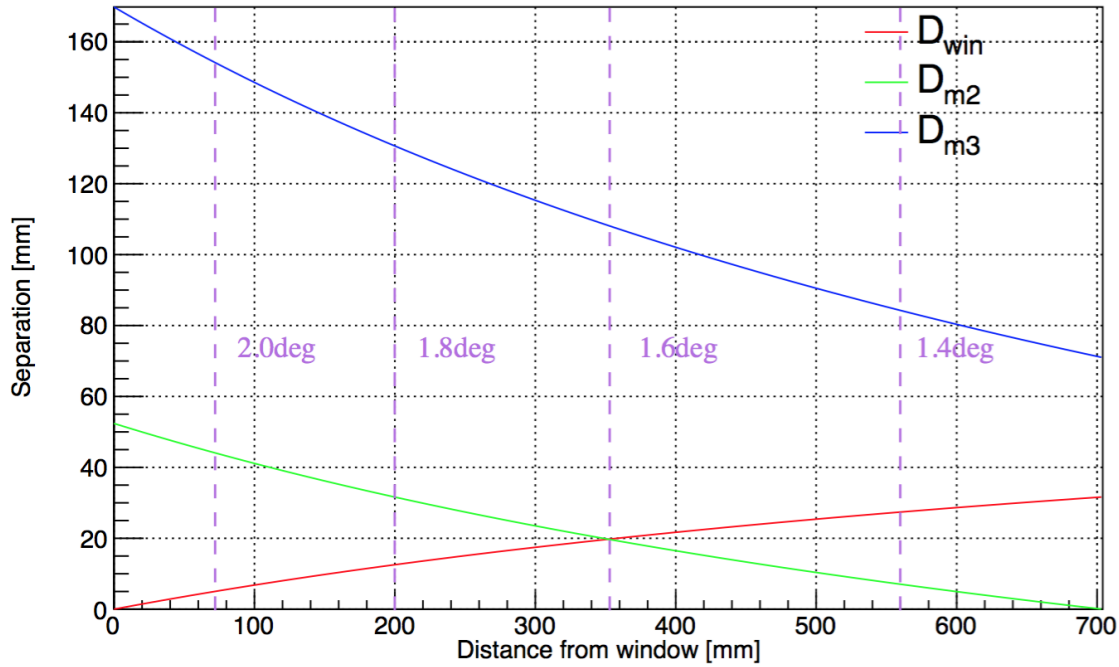


FIGURE 3.11: .

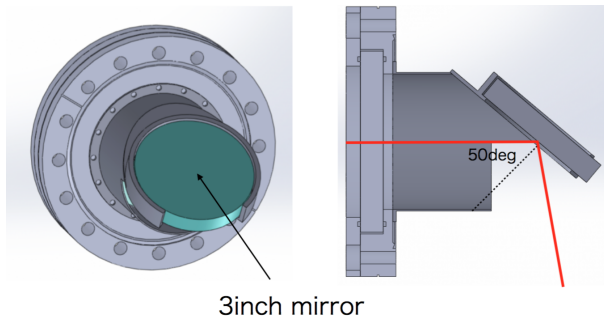


FIGURE 3.12: .

periscope at the vacuum side of the window because we should avoid optical lever path. We set the incident angle of periscope mirror as 50 degrees.

The flange type of the view port is ICF152. We remodeled the blank flange of ICF 152 made by Cosmotech. Figure 3.12 shows the drawing of the view port. We employ the G-85 o-ring for vacuum sealing.

3.3.3 Mirrors

We employ eight 3 inch mirrors. We place the HR coating on the polished fused silica disc. The coating and polishing the fused silica is made by Sigma-koki corporation. The reflectance of the mirror is shown in Figure. XXXX. The reflectance of HR coating depends on the incident angle and the polarization angle. We labeled mirrors as M1, XXXX. The specification of mirrors are summarized in Table. 3.10. All mirror is aligned with optical mirror mount made by XXXXXX.

TABLE 3.10: Specification of Mirrors in periscope.

Mirror number	part number	Diameter [mm]	Incident angle	Polarization
M-P-1		76.2	50deg	
M-P-2		76.2	50deg	
M-P-t-3		76.2	22.5deg	
M-P-t-4		76.2	45deg	
M-P-b-3		76.2	22.5deg	
M-P-b-4		76.2	45deg	
M-P-5		76.2	50deg	
M-P-6		76.2	50deg	

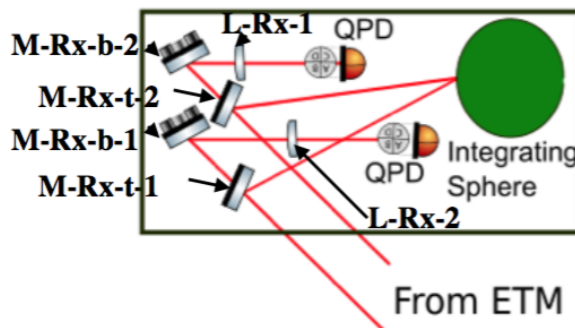


FIGURE 3.13

3.3.4 Structure

3.3.5 Alignment

3.4 Receiver module

3.4.1 6inch Integrating sphere

The 6 inches integrating sphere is used for absolute power measurement of the laser. We receive the laser beam from two paths. To receive the power perfectly, we need a sufficiently large diameter hole of integrating sphere. We use for the 2 inch hole integrating sphere. We mounted the photo detector at the top of port. Details of the photo detector is explained in Sec. 3.2.10.

3.4.2 Mirror

We employ four 2 inch mirrors. We place the HR coating made by Siguma-koki as shown in Fig. XXXX. For two mirrors, we make the AR coating on the back surface to pick up the beams. The specification of the mirrors are listed in Table 3.11.

3.4.3 QPD

We will implement QPDs for beam position control, which made by Thorlabs. They also help us to understand the alignment drifts of the beams. The part number of QPD is PDQ30C.

TABLE 3.11: Specification of Mirrors in Rx module.

Mirror number	part number	Diameter [mm]	Incident angle	Polarization
M-Rx-1		76.2	21.7deg	
M-Rx-2		76.2	23.3deg	
M-Rx-3		76.2	21.7deg	
M-Rx-4		76.2	23.3deg	

TABLE 3.12: Specification of QPD.

Charactaristic	Typical value	Unit	Note
Substrate	InGaAs		
Wavelength Range	1000 - 1700	nm	
Detector Bandwidth	150	kHz	
Recommended Spot Size	ϕ 0.2 - 0.5	mm	

3.4.4 Structure

The breadboard is placed on the support structure. The material of this structure is SUS 306. We simulated the resonance frequency using ANSYS. The estimated frequency is XXX Hz.

3.5 Camera module

The beam position of the ETM surface corresponds to systematic error of the rotation and elastic deformation. To measure the beam position, we measure the mirror surface directly. However, the KAGRA EXA/EYA chambers are placed at 36m far from the ETM. Thus, we employ the combination of telescope and high resolution camera, we call telephoto camera (TCam). We are tuning with focus point of the mirror using focuser. We place the view port and mirror between the ETM and TCam. Figure 3.14 shows the drawing of TCam unit.

3.5.1 Camera

Purpose of using the high resolution camera, we have to measure the beam position within 1 mm accuracy. We solved this problem by D810 digital camera made by Nikon. The D810 reprises the 36-megapixel resolution with 35.9×24.0 mm CMOS sensor. We remove the IR filter because the commercial camera is not sensitive to laser wavelength (1047 nm).

3.5.2 Telescope

We employ the Maksutov-Cassegrain type telescope for observing the ETM surface. The diameter of the primary mirror is 127 mm and its focal length is 1500 mm ($f/12$). The telescope is manufactured by Sky-watcher company. The diameter of the telescope is limited by the that of the view window size.

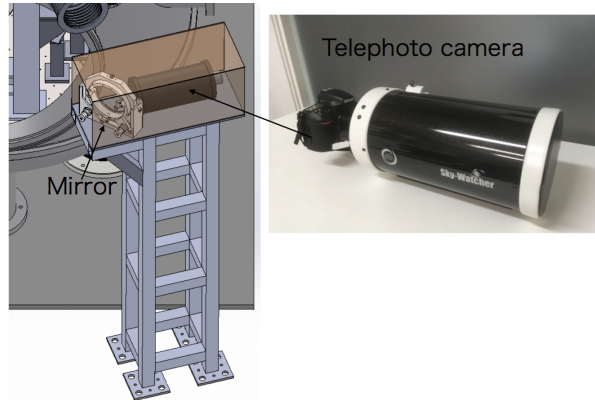


FIGURE 3.14: .

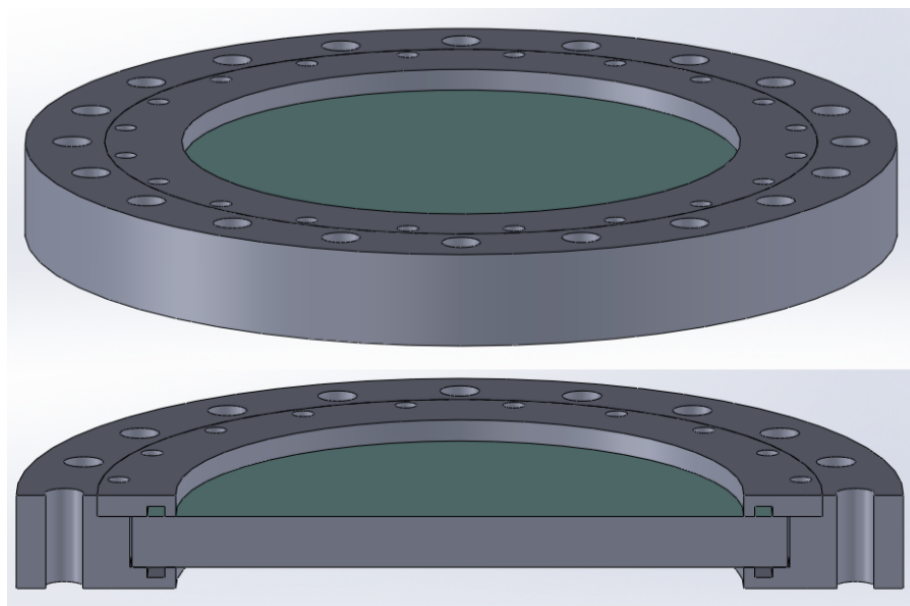


FIGURE 3.15: .

3.5.3 Focuser

A focuser, which is made by Moonlight, is used for the automatic focus control. We connect focuser between telescope and camera. The model number is XXXXX.

3.5.4 View window

The flange type of the view port is ICF203. We remodeled the blank flange of ICF 203 made by Cosmotech. Figure 3.15 shows the drawing of the view port. We employ the G-135 o-ring for vacuum sealing.

3.5.5 Mirror

We place the mirror in the EXA/EYA chamber. The mirror size is $100 \times 80\text{mm}$, which is mounted on the aluminum holder and optical mount. The mirror is made by Thorlab. The reflectance of the mirror is shown in Fig XXXX.

3.5.6 Illuminator

3.6 Summary

Chapter 4

Elastic deformation

The elastic deformation is one of the serious systematic error in Photon calibrator.

4.1 Free mass motion

4.2 Transfer function

4.3 Modal analysis

4.4 Elastic deformation

4.5 Summary

Chapter 5

Absolute power calibration

5.1 Introduction

This section describes the in-situ calibration procedure of Photon Calibrator at each End station of KAGRA.

5.2 Theory of Operation

The Working Standard referred as WS is an integrating sphere with InGaAs photo detector, which has been calibrated against Gold Standard (GS) in the lab at LHO. The Gold Standard is calibrated by NIST. We will use this working standard to calibrate the Transmitter Module Photo Detector (TxPD) and Receiver Module Photo detector (RxPD), which are inside the Transmitter module and Receiver module of Photon calibrator respectively.

The following formula is used to obtain the calibration factor that will give the response of photodiodes in Photon calibrator modules in Watts/Volts:

$$\text{TxPD} = \frac{\text{TX}}{\text{WS}} * \frac{\text{WS}}{\text{GS}} * \text{GS} \quad (5.1)$$

$$\text{RxPD} = \frac{\text{RX}}{\text{WS}} * \frac{\text{WS}}{\text{GS}} * \text{GS} \quad (5.2)$$

5.3 End-station

5.4 Gold standard

5.5 Working standard

Chapter 6

Beam position monitor

Chapter 7

Discussion

Chapter 8

Summary

Bibliography

- ¹B. P. Abbott, et al., “Observation of Gravitational Waves from a Binary Black Hole Merger”, [Phys. Rev. Lett. 116, 061102 \(2016\)](#).
- ²B. P. Abbott, et al., “GW151226: Observation of Gravitational Waves from a 22-Solar-Mass Binary Black Hole Coalescence”, [Phys. Rev. Lett. 116, 241103 \(2016\)](#).
- ³S. Klimenko, G. Vedovato, M. Drago, G. Mazzolo, G. Mitselmakher, C. Pankow, G. Prodi, V. Re, F. Salemi, and I. Yakushin, “Localization of gravitational wave sources with networks of advanced detectors”, [Phys. Rev. D83, 102001 \(2011\)](#).
- ⁴B. P. Abbott, et al., “Calibration of the Advanced LIGO detectors for the discovery of the binary black-hole merger GW150914”, [arXiv 1602, 03845 \(2016\)](#).
- ⁵S. Karki, et al., “The Advanced LIGO Photon Calibrators”, [Rev. Sci. Instrum. 87, 114503 \(2016\)](#).
- ⁶L. Rolland, F. Marion, and B. Mours, “Conceptual design of advanced virgo photon calibration”, [Virgo TDS 0013A, 15 \(2015\)](#).
- ⁷T. Accadia, et al., “Reconstruction of the gravitational wave signal $h(t)$ during the Virgo science runs and independent validation with a photon calibrator”, [Class. Quant. Grav. 31, 165013 \(2014\)](#).
- ⁸D. A. Clubley, G. P. Newton, K. D. Skeldon, and J. Hough, “Calibration of the Glasgow 10-m prototype laser interferometric gravitational wave detector using photon pressure”, [Phys. Lett. A283, 85–88 \(2001\)](#).
- ⁹K. Mossavi, M. Hewitson, S. Hild, F. Seifert, U. Weiland, J. R. Smith, H. Luck, H. Grote, B. Willke, and K. Danzmann, “A photon pressure calibrator for the GEO 600 gravitational wave detector”, [Phys. Lett. A353, 1–3 \(2006\)](#).
- ¹⁰E. Goetz, et al., “Precise calibration of LIGO test mass actuators using photon radiation pressure”, [Class. Quant. Grav. 26, 245011 \(2009\)](#).
- ¹¹B. Mours, and L. Rolland, “Determining the sign of h-rec with the photon calibrator”, [Virgo TDS 018A, 07 \(2007\)](#).
- ¹²B. P. Abbott, et al., “Prospects for observing and localizing gravitational-wave transients with advanced ligo and advanced virgo”, [Living Reviews in Relativity 19, 1 \(2016\)](#).
- ¹³M. Ando, “Observation Scenario Paper”, [JGW G1706116 \(2017\)](#).